A Finite Element Method for the Boundary Data Recovery in an Oxygen-Balance Dispersion Model

Faker Ben Belgacem, Naima Debit, Henda El Fekih, Souad Khiari

A Finite Element Method for the Boundary Data Recovery in an Oxygen-Balance Dispersion Model

Faker Ben Belgacem* Naïma Débit† Henda El Fekih‡ Souad Khiari§ ¶

July 12, 2014

Abstract

The inverse problem under investigation consists of the boundary data completion in a deoxygenation-reaeration model in stream-waters. The unidimensional transport model we deal with is based on the one introduced by Streeter and Phelps, augmented by Taylor dispersion terms. The missing boundary condition is the load or/and the flux of the biochemical oxygen demand indicator at the outfall point. The counterpart is the availability of two boundary conditions on the dissolved oxygen tracer at the same point. The major consequences of these non-standard boundary conditions is that dispersive transport equations on both oxygen tracers are strongly coupled and the resulting system becomes ill-posed. The main purpose is a finite element space-discretization of the variational problem put under a non-symmetric mixed form. Combining analytical calculations, numerical computations and theoretical justifications, we try to elucidate the characteristics related to the ill-posedness of this data completion dynamical problem and understand its mathematical structure.

KEYWORDS: Dispersive transport, Data completion, Ill-posedness, Mixed finite elements, Differential algebraic equations.

*Sorbonne Universités, Université de Technologie de Compiègne, LMAC, EA 2222, F-60205 Compiègne, France and CNRS, I2M, UMR5295, 33607 Pessac Cedex, France..

†Université de Lyon, CNRS, Université Lyon 1 ; Institut Camille Jordan, UMR5208, F-69622 Villeurbanne Cedex, France

‡Université de Tunis El Manar, Ecole Nationale d'Ingénieurs de Tunis, LAMSIN, 1002, Tunis, Tunisie

§Sorbonne Universités, Université de Technologie de Compiègne, LMAC, EA 2222, F-60205 Compiègne, France.

¶Université de Tunis El Manar, Ecole Nationale d'Ingénieurs de Tunis, LAMSIN, 1002, Tunis, Tunisie

1 Introduction and setting of the inverse problem

The analysis of the oxygen household conditions is central in the water quality modeling. Aquatic life and ecosystem are strongly dependent on the oxygen content of stream-waters. The oxygen balance is governed by the deoxygenation-reaeration problem which is composed of two dispersive transport scalar equations. One involves the biochemical oxygen demand (BOD) concentration and the other is the dissolved oxygen (DO) density. After the mixing length is over practitioners may have good reasons for considering one dimensional models. Our investigation is actually based on oneD problem. Throughout, we denote $I = (0, L)$ the curvilinear representation of the stream-water and $T > 0$ is a final instant. We use the symbol x for the curvilinear abscissa and t stands for the time variable. The linear dispersive transport system describing the oxygen balance reads therfore as

$$\begin{aligned} \partial_t b - (db' + vb)' + rb &= f \qquad \text{in } I \times (0,T) \\ \partial_t c - (dc' + vc)' + r_* c + rb &= g \qquad \text{in } I \times (0,T) \\ db'(L,t) = dc'(L,t) &= 0 \qquad\qquad \text{in } (0,T) \\ b(x,0) = b_0(x), \quad c(x,0) &= c_0(x) \qquad\qquad \text{in } I. \end{aligned} \tag{1}$$

The longitudinal dispersion coefficient d, the average flow velocity v and the parameters of reaction rates (r, r_*) are all in $L^\infty(I)$. Moreover d, r and r_* are positive and are assumed to be piecewise continuous on $\overline{I}$. The dispersion parameter is also bounded away from zero. There exists a constant $\underline{d} > 0$ such that $d(x) > \underline{d}$. We assume also that $r(x) > \underline{r} > 0$. The space-time dependent function b denotes the biochemical oxygen demand concentration and c is the dissolved oxygen. One dimensional models are currently used when one is interested in the downstream dispersion and propagation of an accidental pollution (see [15, 5, 10]). The term rb appearing in the transport equation on c is the depletion of oxygen. This oxygen fraction is necessary to the micro-organisms to oxidize the excessive biodegradable matter in the water. Let us point out that if the dispersion terms are canceled in both transport equations, we obtain the famous Streeter-Phelps model (see [19]).

Zero Neumann boundary conditions at point $x = L$ say that there is no polluting flux downstream. When every thing is known, suitable boundary conditions are given at the outfall point $(x = 0)$ on both concentrations b and c. They may have the following form

$$b(0,t) = \eta(t), \qquad -dc'(0,t) = 0 \qquad \text{in } (0,T). \tag{2}$$

No oxygen supply occurs at the outfall point $x = 0$ and the polluting load at that same point is known and fixed to $\eta(\cdot)$. Most often they are of Neumann type,

$$-db'(0,t) = \gamma(t), \qquad -dc'(0,t) = 0 \qquad \text{in } (0,T). \tag{3}$$

This tells that a polluting flux γ is taking place at $(x = 0)$. That flux may have various causes. It may for instance be originated from an accidental spill upstream of the river portion under

investigation or may be the result of drainage of fertilizers from farm fields. Notice that we are interested in the health state of the river portion downstream. From the modeling point of view, it sounds reasonable, although not necessary from the mathematical view, to consider that the advection velocity is such that $v < 0$ at least at the vicinity of $x = 0$. The river flow then inside I at $x = 0$.

The direct system (1) and (2) (or (3)) is weakly coupled. It is in fact triangular and can be studied using well known tools from the theory of parabolic differential equations (see [16, 14]). The specific fact here is that, in real-life situations, measurements on the polluting load η or flux γ are too hard to obtain. In the contrary, recording the values of c at the border is easy and may be realized instantaneously. Conditions (2) (or (3)) are therefore replaced by both Dirichlet and Neumann conditions on c,

$$c(0,t) = \alpha(t) \qquad -dc'(0,t) = 0 \qquad \text{in } (0,T). \tag{4}$$

The effect of the modification of the boundary conditions on the problem is dramatic. The nature of the problem is entirely altered. With (3), it was well posed, with (4) it becomes ill-posed. It was weakly coupled, it becomes strongly coupled through the boundary conditions. It was a direct problem it becomes an inverse problem. One has for instance to reconstruct the polluting flux γ from a supplementary Dirichlet condition on c at $x = 0$.

The study realized for this inverse problem in [1] provides a brief illustration of the instability of the (hypothetic) solution with respect to the data. We propose here to conduct a deeper investigation, in Section 2 to accurately quantify the ill-posedness degree as defined in [22]. Understanding the mathematical structure of this dynamical system becomes troublesome. An identifiability result has been proved in [1]. Calling for the open map theorem in a suitable framework, one concludes that a by-product of the instability and the uniqueness is that the existence of the solution can not succeed for arbitrary data. The purpose here is to realize a space approximation of the inverse problem (1) and (4) by a finite element method. The semi-discrete problem turns out to be a differential algebraic equation. We check out how it is affected by the ill-posedness. In particular, the existence issue is tackled frontally owing to the Weierstrass-Kronecker canonical decomposition. This is the subject of Sections 3 and 4. In Section 5, we suggest a full discretization by advancing in time using the Euler scheme. We discuss some issues about the properties of the full discrete problem. To end, we present in Section 6 some numerical experiences to assess the computing devices we use in the simulation of the inverse problem we deal with.

2 Ill-posedness degree and Uniqueness

A wide literature exists dealing with the direct problem (1) and (3) in both theoretical and computational registers. To our opinion, putting aside the non-linearities not provided here, the most

important feature that has been studied has to do with the influence of the Péclet number on the numerical simulations (see, eg, [18]). The specific issue we are confronted to in this work is related to the redundancy of the boundary condition on the concentration c at $x = 0$ to compensate the lack of conditions on the density b. With this respect, the dispersion plays a preponderant role in the complications arisen in the mathematical handling of the inverse problem. We will therefore exclusively focus in this effect. As shown in [1] and this will be confirmed along this work, the study is far from being easy to achieve and we thus prefer to switch off any further causes of technical difficulties so as to stress on the central issue.

The ill-posedness of the problem has been briefly illustrated in [1]. We here intend to accurately evaluate the ill-posedness degree, as defined in [22], at the cost of a more complete investigation. We accomplish this study when the physical parameters are all constants. According to the remark made above, the main point is the incidence of the dispersion. To simplify, one may get rid of the advection. Indeed, as well known in the theory of Sturm-Liouville operators, there is a suitable transformation that allows to hide the advective term. In addition, the most important feature is concerned with the sensitivity of the reconstructed flux $\gamma(\cdot)$ in (3) with respect to the measures $\alpha(\cdot)$ in (4). To alleviate the exposition, we fix (f, g) and (b_0, c_0) to zero. This is not a restriction to generality. Henceforth, we assume that $v = 0$ in both transport scalar equations on b and c. Since we intend to use Fourier series we put $L = \pi$ to alleviate the calculations. We therefore consider the pure dispersion-reaction problem

$$\begin{aligned}
\partial_t b_\gamma - d b''_\gamma + r b_\gamma = 0 \qquad & \text{in } I \times (0,T) \\
\partial_t c_\gamma - d c''_\gamma + r_* c_\gamma + r b_\gamma = 0 \qquad & \text{in } I \times (0,T) \\
d b'_\gamma(\pi,t) = d c'_\gamma(\pi,t) = 0 \qquad & \text{in } (0,T) \\
-d b'_\gamma(0,t) = \gamma(t), \quad -d c'_\gamma(0,t) = 0 \qquad & \text{in } (0,T) \\
b_\gamma(x,0) = 0, \quad c_\gamma(x,0) = 0 \qquad & \text{in } I.
\end{aligned} \tag{5}$$

The polluting agent is the flux $\gamma(\cdot)$. The right one to recover is the one that yields the observations $\alpha(\cdot)$. It is thus solution of the following reduced equation

$$(S\gamma)(t) := c_\gamma(0,t) = \alpha(t) \qquad \text{in } (0,T). \tag{6}$$

If $\gamma(\cdot)$ is given then the direct system (5) is triangular and has a unique solution (b_γ, c_γ). The linear operator S is well defined and maps continuously $L^2(0,T)$ into $L^2(0,T)$. Using Fourier series in (5), S can be expressed as a convolution operator. Indeed, assembling the dispersion-reaction equation, the boundary and the initial conditions on b_γ, then solving the well-posed resulting problem, one obtain that

$$b_\gamma(x,t) = \frac{1}{\pi}\int_0^t \gamma(s) e^{-r(t-s)}\, ds + \frac{2}{\pi}\sum_{k\geq 1}\Big(\int_0^t \gamma(s) e^{-\lambda_k (t-s)}\, ds\Big)\cos(kx).$$

The sequence $(\lambda_k)_k$ is given by $\lambda_k = dk^2 + r$. In the other hand side, gathering the equation on c and due to the Neumann boundary and initial conditions it may be stated that

$$c_\gamma(x,t) = \frac{r}{\pi}\int_0^t \gamma(s)e^{-r_*(t-s)}\left[\frac{1-e^{-(r-r_*)(t-s)}}{r-r_*}\right]ds + \frac{2r}{\pi}\sum_{k\in\mathbb{N}}\Big(\int_0^t \gamma(s)e^{-\mu_k(t-s)}\left[\frac{1-e^{-(r-r_*)(t-s)}}{r-r_*}\right]ds\Big)\cos(kx).$$

Here, we have $\mu_k = dk^2 + r_*$. Now, considering $c_\gamma(0,t)$, this formula yields the convolution form of S, that is

$$(S\gamma)(t) = \int_0^t K(t-s)\gamma(s)\,ds \qquad \forall t \in (0,T).$$

The convolution kernel $K(\cdot)$ is given by

$$K(s) = \frac{r}{\pi(r-r_*)}(1-e^{-(r-r_*)s})\Big(e^{-r_*s} + 2\sum_{k\geq 1} e^{-\mu_k s}\Big) \qquad \forall s \in (0,T).$$

It is easily seen that K is indefinitely smooth away from the origin. The qualitative properties of S are thus tightly dependent on the behavior of this kernel at the vicinity of zero. By the way, a useful information one can have right away is the ill posedness of problem (6) because of $K(0) = 0$. In particular, the operator S is compact. We aim to know more about the ill-posedness degree of (6). This may be ensued from the asymptotics of the singular values of the operator S (see [9]). We are hence required to find out the positive real number $a > 0$ so that $K(s) = \mathcal{O}(s^a)$. This pertains to the limit toward zero of the infinite sum defining $K(\cdot)$. Comparison with integrals allows to state that

$$K(s) \sim -\frac{r}{2\sqrt{\pi d}}\sqrt{s},$$

at the vicinity of zero. Applying Theorem 3.1 proved in [7], concludes to the fact that the sequence of the singular values of the operator S decays towards zero like $Ck^{-3/2}$. This tells that the ill-posedness degree is 3/2 and ascertains of the mild ill-posedness of the reduced problem (6). As a result, the resolvent of the inverse problem (1) and (4) cannot be continuous and that problem suffers thus from instability.

Remark 2.1 *One may wonder why the data completion problem we consider is mildly ill-posedness. A fundamental part of the answer is the fact that the reconstruction of the missing pollution flux $\gamma(\cdot)$ is pursued at the same location where the observations on the oxygen concentration c are made. It may occur of course that collecting measures on c is not possible at that same point $x = 0$ while they are available at a different location. We refer to Figure* 1 *for an illustration*

Let us then have a look at case where the abundant measures on c are obtained at the other extreme point $x = \pi$. The same Fourier computations can be achieved that yields the convolution kernel

$$H(t) = \frac{r}{\pi(r-r_*)}(1-e^{-(r-r_*)s})\Big(e^{-r_*s} + 2\sum_{k\geq 1}(-1)^k e^{-\mu_k s}\Big) \qquad \forall s \in (0,T).$$

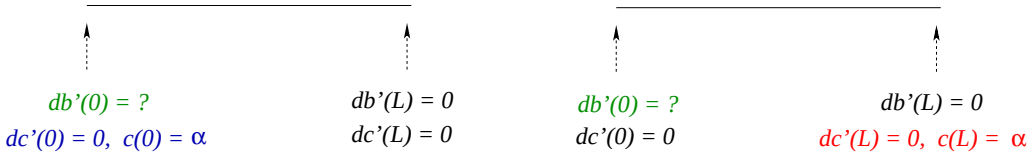

Figure 1: Data can be collected either at of the outfall point or downstream.

The sign $(-1)^k$ *in the infinite sum brings a dramatic change on the behavior of the kernel at the vicinity of zero. Both kernels* $K(\cdot)$ *and* $H(\cdot)$ *are plotted in Figure* 2 *when* $d = 1$ *and* $r = r_* = 1$*. The panel to the ledt shows that although* $K(\cdot)$ *vanishes at* $t = 0$ *it is not fat. In the contrary* $H(\cdot)$*, represented in the right panel seem flat at* $x = 0$*. It is really flat, all the derivative of* $H(\cdot)$ *are flat at the origin. This is an indication of severe ill-posedness of the corresponding data completion problem.*

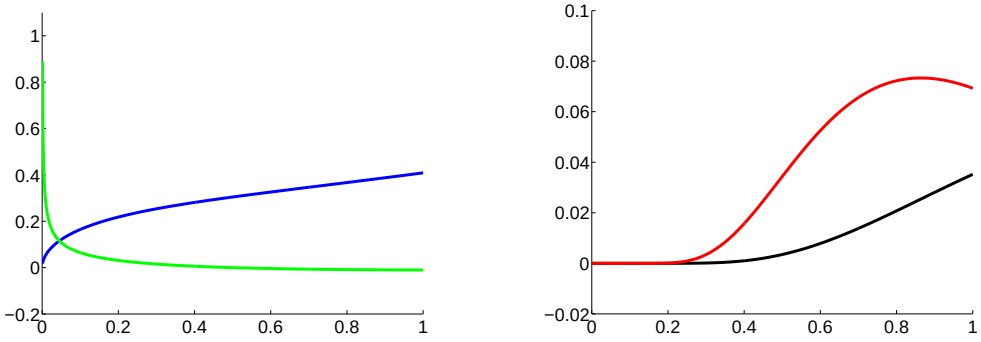

Figure 2: $K(\cdot)$ (left) and $H(\cdot)$ (right) so as their first derivatives on the time interval $(0, 1)$.

The other important issue for the inverse problem has to do with the uniqueness or in other words it is related to the injectivity of S. The result has been established in [1, Theorem 2.7] in the general context of space-varying parameters. The tools used there come from functional analysis of the saddle point problems and are long to summarize. Nevertheless, it may be briefly discussed in some particular cases. We intend to provide an illustration of that uniqueness result using a simple argument. We then consider the same problem as above. The parameters are all constant and we make the additional assumption that $T = \infty$. We are consequently enabled to use Laplace's transform as a bounded operator in $L^2(0, \infty)$. The reduced problem, where $\alpha(\cdot)$ is put to zero, can then be written as

$$\widehat{S\gamma}(p) = \hat{K}(p)\hat{\gamma}(p) = 0 \qquad \forall p \in (0, \infty).$$

The symbol $\hat{\gamma}(\cdot)$ is for the Laplace transform of the function $\gamma(\cdot)$. Easy computation yields that

$$\hat{K}(p) = \frac{2r}{\pi} \sum_{k\in\mathbb{N}} \frac{1}{(p+\mu_k)(p+\lambda_k)} \qquad \forall p \in (0,\infty).$$

It can be checked out that $\hat{K}(p) \neq 0, \forall p \in (0,\infty)$, we derive that $\hat{\gamma}(\cdot)$ vanishes identically. On account of the injectivity of the Laplace transform we conclude to $\gamma(\cdot) = 0$. The uniqueness is assessed by linearity.

Before closing this section let us say some words about the surjectivity of S which has a narrow link to the existence for problem (6). Let us first indicate that the adjoint operator S^* is an integral operator. Following the same arguments as for S, it can be proved that S^* is injective. The range of S is thus dense in $L^2(0,\infty)$ and cannot be closed. Otherwise, applying the open map theorem yields that the inverse of S would be bounded, but we known that it is not. Hence, surjectivity fails for S and the existence of a solution for (6) may not be ensured. The same conclusion may be extended to problem (1) and (4).

3 Finite element approximation

A space finite element approximation of the problem (1) and (4) is the purpose here. As we will see later on this sheds more clarity about the existence issue which was addressed through an indirect argument for the continuous problem. We still keep the assumption, $v = 0$. Moreover, handling non-homogeneous Dirichlet conditions does not arise any particular obstacle. We assume thus that $\alpha(\cdot)$ is also zero. Adding the advection in the inverse model or/and taking into account non-vanishing boundary condition do not introduce more complexity from the theoretical point of view, even though they are undeniably important in the physical and computational grounds.
Let $I_i = (x_i, x_{i+1})_{1\leq i\leq n-1}$ be a subdivision of the interval I with $x_1 = 0$ and $x_n = \pi$. The grid-size h is equal to $\max_{1\leq i\leq n-1} |I_i|$. We refer to [4, 6] for the basics of the finite element method. Next, we define the discrete spaces V_h and H_h

$$V_h = \Big\{\varphi_h \in \mathscr{C}(I); \quad \forall i,\ (\varphi_h)_{|I_i} \in \mathcal{P}_1\Big\},$$
$$H_h = \Big\{\psi_h \in \mathscr{C}(I); \quad \forall i,\ (\psi_h)_{|I_i} \in \mathcal{P}_1,\ \psi_h(0) = 0\Big\},$$

where $\mathcal{P}_1$ stands for the space of affine functions. The space approximation relies on a mixed variational form of the problem. The framework selected here reproduces the one used in [1], adapted to the discrete level. That framework is the only one liable to provide the identifiability result for the exact model (1) and (4). It sounds natural to select it for our finite element approximation.
The semi-discrete problem is hence constructed following Ritz–Galerkin's procedure. It reads as:

find (b_h, c_h) *in* $V_h \times H_h$ *fulfilling*

$$\begin{aligned} &\forall \psi_h \in H_h, \qquad (\partial_t b_h(t), \psi_h)_{L^2(I)} + k\,(\psi_h, b_h(t)) = (f(t), \psi_h)_{L^2(I)}, \\ &\forall \varphi_h \in V_h, \qquad (\partial_t c_h(t), \varphi_h)_{L^2(I)} + k_*(c_h(t), \varphi_h) + a_r(b_h(t), \varphi_h) = (g(t), \varphi_h)_{L^2(I)}, \\ &\qquad\qquad b_h(\cdot, 0) = b_{0,h}, \quad c_h(\cdot, 0) = c_{0,h}. \end{aligned} \tag{7}$$

Using $(\cdot,\cdot)_{L^2(I)}$ marks the inner product in the space $L^2(I)$. Different bilinear forms $k(\cdot,\cdot)$ and $k_*(\cdot,\cdot)$ and $a_r(\cdot,\cdot)$ are expressed by,

$$\begin{aligned} \forall (\psi_h, \varphi_h) \in H_h \times V_h, \qquad & k(\psi_h, \varphi_h) = \int_I (d b_h' \psi_h' + r b_h \psi_h)\, dx, \\ \forall (\psi_h, \varphi_h) \in H_h \times V_h, \qquad & k_*(\psi_h, \varphi_h) = \int_I (d c_h' \psi_h' + r_* c_h \psi_h)\, dx, \\ \forall (\psi_h, \varphi_h) \in V_h \times V_h, \qquad & a_r(\chi_h, \varphi_h) = \int_I r \chi_h \varphi_h\, dx. \end{aligned}$$

To put the mixed problem under a matrix form, we denote by $\boldsymbol{b}$ and $\boldsymbol{c}$ the vectors of unknowns for the concentration b_h and the density c_h, respectively. The degrees of freedom in $\boldsymbol{b}$ are the values of b_h at all grid vertices and those of $\boldsymbol{c}$ made of the values of c_h at all the vertices except at $x_1 = 0$ where c_h vanishes. Problem (7) can be expressed under a matrix form,

$$\begin{pmatrix} \tilde{M} & 0 \\ 0 & \tilde{M}^T \end{pmatrix} \partial_t \begin{pmatrix} \boldsymbol{b}(t) \\ \boldsymbol{c}(t) \end{pmatrix} + \begin{pmatrix} K & 0 \\ A_r & K_*^T \end{pmatrix} \begin{pmatrix} \boldsymbol{b}(t) \\ \boldsymbol{c}(t) \end{pmatrix} = \begin{pmatrix} \boldsymbol{f}(t) \\ \boldsymbol{g}(t) \end{pmatrix}, \qquad \text{in } (0,T).$$

The symbol ^{T} is for the transposition. The matrix A_r, of type (n,n), is linked to $a_r(\cdot,\cdot)$ and coincides with the mass matrix with respect to the weight r. It is symmetric positive definite. The notation $\tilde{M}$ is for the rectangular mass matrix of type $(n, n-1)$. It is extracted from the full mass matrix representing the L^2-inner product in V_h. K and K_* stand for the stiffness matrices related to the mixed bilinear forms $k(\cdot,\cdot)$ and $k_*(\cdot,\cdot)$, respectively. They are rectangular, of type $(n, n-1)$. Moreover, the obvious coerciveness of both $k(\cdot,\cdot)$ and $k_*(\cdot,\cdot)$ on the space $H_h \times H_h$ yields that the matrices K and K_* are full rank matrices. Consequently their transposes K^T and $(K_*)^T$ are injective. To put the discrete problem under a compact form we list all the degrees of freedom in a single vector called $\boldsymbol{Y}$. This vector contains therefore $(2n-1)$ degrees of freedom and is solution of the initial value problem

$$\begin{aligned} \boldsymbol{M}\, \partial_t \boldsymbol{Y}(t) + \boldsymbol{K}\boldsymbol{Y}(t) &= \boldsymbol{G}(t), \qquad \text{in } (0,T) \\ \boldsymbol{Y}(0) &= \boldsymbol{Y}_0. \end{aligned} \tag{8}$$

The data $\boldsymbol{G}$ contains the contribution of the input $(\boldsymbol{f}, \boldsymbol{g})$ and $\boldsymbol{Y}_0$ contains the initial states $(\boldsymbol{b}_0, \boldsymbol{c}_0)$. Both matrices $\boldsymbol{M}$ and $\boldsymbol{K}$ are square. Problem (8) is an implicit differential equation; it is not an ordinary differential equation because $\boldsymbol{M}$ is not invertible. The incidence of this singularity is that existence for (8) may fail for arbitrary data.

4 A differential algebraic system

Understanding the particular structure of equation (8) is tightly connected to the matrix $\boldsymbol{M}$. Let us therefore check out the important statement

The kernel $\mathcal{N}(\boldsymbol{M})$ is a subspace of dimension one. The matrix $\boldsymbol{M}$ is therefore singular.

Proof : Let $\boldsymbol{Y}$ be given in $\mathcal{N}(\boldsymbol{M})$. We consider $(b_h, c_h) \in V_h \times H_h$ as the finite element functions whose degrees of freedom form the coefficients of $\boldsymbol{Y}$. According to the construction of $\mathcal{N}(\boldsymbol{M})$, the following double orthogonality holds

$$\int_I b_h \psi_h \, dx = 0, \qquad \forall \psi_h \in H_h; \qquad\qquad \int_I c_h \varphi_h \, dx = 0, \qquad \forall \varphi_h \in V_h. \tag{9}$$

We deduce directly that $c_h = 0$. The function b_h considered alone has n degrees of freedom. It is subjected to $(n-1)$ constraints that are linearly independent. As a consequence, the set of these functions determines a vector space of dimension one. The value $b_h(x_1)$ can be considered as the only degree of freedom. The dimension of the kernel $\mathcal{N}(\boldsymbol{M})$ is thus one. This results in the non-invertibility of $\boldsymbol{M}$.

Remark 4.1 *The dimension of $\mathcal{N}(\boldsymbol{M})$ depends in fact upon the boundary points where Cauchy's conditions are enforced on the density c. If they are also prescribed at point $x = \pi$, the dimension of $\mathcal{N}(\boldsymbol{M})$ becomes two.*

As a consequence of the non-invertibility of $\boldsymbol{M}$, problem (8), apparently a differential equation, is actually hiding an algebraic and a differential (sub)equations or components. It is a differential algebraic equation. An exposition of these of equations may be found in some manuscripts (see [12, 13, 17, 3]) where specific tools are elaborated to cope with them. Before proceeding with this methodology, it is useful to know more about the stiffness matrix $\boldsymbol{K}$. It turns out to be invertible under a mild assumption on the grid-size. This condition on the mesh is liable to ensure the discrete positivity principle. Observe first that the kernel of the matrix K can be identified to the subspace

$$\mathcal{N}(K) = \big\{\varphi_h \in V_h; \quad k(\psi_h, \varphi_h) = 0, \forall \psi_h \in Q_h\big\}.$$

The subspace $\mathcal{N}(K_*)$ in linked to $k_*(\cdot,\cdot)$ in the same way. Under the condition on the grid-size

$$h^2 \max\,(\sup_{x\in I} r(x), \sup_{x\in I} r_*(x)) \leq 6 \inf_{x\in I} d(x), \tag{10}$$

the following statement holds true (see [21])

$$\varphi_h \in \mathcal{N}(K) \cap \mathcal{N}(K_*), \quad \varphi_h(0) \geq 0 \quad \text{implies that} \quad \varphi_h(x) \geq 0, \forall x \in I.$$

We have thence the invertibility result,

Assume condition (10) *on the grid-size is fulfilled. Then, the stiffness matrix* $\boldsymbol{K}$ *is invertible.*

Proof : Let $\boldsymbol{Y}$ be in $\mathcal{N}(\boldsymbol{K})$ and is the representation of (b_h, c_h). It is direct that $b_h \in \mathcal{N}(K)$. Moreover, it can be easily checked out that

$$a_r(b_h, \varphi_h) + k_*(\varphi_h, c_h) = a_r(b_h, \varphi_h) = 0, \qquad \forall \varphi_h \in \mathcal{N}(K_*).$$

Choosing φ_h such that $\varphi_h(x_1) = b_h(x_1)$, then, by the positivity principle both b_h and φ_h are simultaneously positive or negative. The fact that $a_r(b_h, \varphi_h) = 0$ results in $b_h = \varphi_h = 0$. Deducing that $c_h = 0$ becomes straightforward from the injectivity of $(K_*)^T$. We conclude thus to $\boldsymbol{Y} = 0$, hence the proof.

Remark 4.2 *Arguing analogously, one can also obtain that* $(\lambda \boldsymbol{M} + \boldsymbol{K})$ *is invertible for any* $\lambda \geq 0$.

To reveal useful properties of problem (8), we call for the algebraic transformation introduced by Kronecker and Weierstrass (see [11, 23]). The chief idea is to put the problem under a canonical 'Weierstrass-Kronecker' form that enables to uncouple the differential equation and the algebraic equation and to find out their respective dimension. Then, each of the two subproblems can be studied in its own context.
Realizing this requires the regularity in the sense of 'Weierstrass-Kronecker'. The matrix pencil formed by the pair of matrices $(\boldsymbol{M}, \boldsymbol{K})$ is regular because the characteristic polynomial $p(\lambda) = \det(\lambda \boldsymbol{M} + \boldsymbol{K})$ does not vanish identically. Indeed, $p(0) \neq 0$, as $\boldsymbol{K}$ is invertible. Due to the singularity of $\boldsymbol{M}$, the degree of the polynomial p is obviously lower than n. The following result holds (see [13, Proposition 1.3] and [12, Theorem 2.7])

There exist two linear bijective transformations $\boldsymbol{Z} = \boldsymbol{L}\boldsymbol{Y} = (\boldsymbol{u}, \boldsymbol{v})^T$ *and* $\boldsymbol{R} = \boldsymbol{H}\boldsymbol{G} = (\boldsymbol{q}, \boldsymbol{r})^T$ *which yield the 'Weierstrass-Kronecker' canonical form given by*

$$\begin{pmatrix} I_{n-m} & 0 \\ 0 & N \end{pmatrix} \partial_t \begin{pmatrix} \boldsymbol{u}(t) \\ \boldsymbol{v}(t) \end{pmatrix} + \begin{pmatrix} W & 0 \\ 0 & I_m \end{pmatrix} \begin{pmatrix} \boldsymbol{u}(t) \\ \boldsymbol{v}(t) \end{pmatrix} = \begin{pmatrix} \boldsymbol{q}(t) \\ \boldsymbol{r}(t) \end{pmatrix}, \qquad \text{in } (0, T). \tag{11}$$

The vectors $\boldsymbol{u}, \boldsymbol{q}$ *and* $\boldsymbol{v}, \boldsymbol{r}$ *are of dimension* $(n-m)$ *and* $m \geq 1$ *respectively. The vector function* $\boldsymbol{u}$ *is the differential variable while* $\boldsymbol{v}$ *is the algebraic variable. The sub-matrix* W *is square of dimension* $(n-m)$ *and the bloc* N *is square of dimension* m *with* N *nilpotent. Recall that the nilpotency index* μ *of* N *is the smallest integer such that* $N^\mu = 0$. *The symbol* I_m *is for the unity matrix of dimension* m. *Equation* (11) *can also be displayed under a condensed form*

$$\boldsymbol{N}\partial_t \boldsymbol{Z}(t) + \boldsymbol{W}\boldsymbol{Z}(t) = \boldsymbol{R}(t), \qquad \text{in } (0, T),$$

with the following relations on the matrices, $\boldsymbol{H}\boldsymbol{N} = \boldsymbol{M}\boldsymbol{L}$ *and* $\boldsymbol{H}\boldsymbol{W} = \boldsymbol{K}\boldsymbol{L}$.

To handle the algebraic differential equation (11) we start by considering the new initial state $\boldsymbol{Z}_0 = \boldsymbol{L}\boldsymbol{Y}_0 = (\boldsymbol{u}_0, \boldsymbol{v}_0)^T$. Then, we derive in one hand side the ordinary differential problem

$$\begin{aligned} \partial_t \boldsymbol{u}(t) + W\boldsymbol{u}(t) &= \boldsymbol{q}(t) \qquad \text{in } (0,T), \\ \boldsymbol{u}(0) &= \boldsymbol{u}_0, \end{aligned} \tag{12}$$

and we obtain in the other hand side the algebraic equation

$$\begin{aligned} N\partial_t \boldsymbol{v}(t) + \boldsymbol{v}(t) &= \boldsymbol{r}(t) \qquad \text{in } (0,T), \\ \boldsymbol{v}(0) &= \boldsymbol{v}_0. \end{aligned} \tag{13}$$

The ordinary differential problem (12) is well posed and has unique solution provided by

$$\boldsymbol{u}(t) = e^{-Wt}\boldsymbol{u}_0 + \int_0^t e^{-W(t-s)}\boldsymbol{q}(s)\, ds, \qquad \text{in } (0,T).$$

Letting aside the initial condition for a while, the solution of the algebraic equation (13) may be computed by induction. There comes out the following expression

$$\boldsymbol{v}(t) = \sum_{1\le j\le \mu-1} (-1)^j N^j \boldsymbol{r}^{(j)}(t), \qquad \text{in } (0,T).$$

This formula indicates that the full algebraic equation may not have a solution unless the initial state $\boldsymbol{v}_0$ and the source data $\boldsymbol{r}$ are consistent. Existence is guaranteed by the fulfillment of the constraint

$$\boldsymbol{v}_0 = \sum_{1\le j\le \mu-1} (-1)^j N^j \boldsymbol{r}^{(j)}(0).$$

In the pratice, computing the Weirstrauss-Kronecker decomposition of equation (8) may be expensive and may not be pursued. Actually, solving (8) is highly sensitive to the nilpotency index μ of the matrix N. It is called the Kronecker index of the matrix pencil $(\boldsymbol{M}, \boldsymbol{K})$. This Kronecker index μ and the dimension m of N are both related to the spectral decomposition of the matrix $\boldsymbol{K}^{-1}\boldsymbol{M}$. We already know that 0 is eigenvalue. If ℓ is its algebraic multiplicity then $\dim N = m$ coincides with the dimension of the characteristic subspace $\mathcal{N}((\boldsymbol{K}^{-1}\boldsymbol{M})^\ell)$. The Kronecker index μ is lower or equal to m. Knowing the value of the index μ for the linear differential algebraic equations is so important. It is a strong indication of the complexity of integrating them. Indexes higher or equal to two are causes of instability and generate tough theoretical and practical difficulties. If that index is one, the principal effect is that the initial value cannot be fixed freely in the algebraic (sub)equation. Notice that the result (11) does not provide the Kronecker index nor the dimension of N. This is rather supplied in

The Kronecker index of the pencil $(\boldsymbol{M}, \boldsymbol{K})$ is one, $\mu = 1$. As a consequence, we have $N = 0$. Moreover, the dimension of N is equal to one, $m = 1$.

Proof : Following [8, Appendix A, Theorem 13], the index μ is one if we show that

$$\mathcal{N}(\boldsymbol{M}) \cap \boldsymbol{K}^{-1}(\mathcal{R}(\boldsymbol{M})) = \{0\}.$$

The symbol $\mathcal{R}(\boldsymbol{M})$ is for the range of $\boldsymbol{M}$. Let $\boldsymbol{Y}$ be in the intersection. On one hand side we have that $\boldsymbol{MY} = 0$ and on the other hand side there exists $\boldsymbol{Z}$ such that $\boldsymbol{KY} = \boldsymbol{MZ}$. Now, denote (b_h, c_h) and (β_h, χ_h) the finite element functions in $V_h \times H_h$ associated to $\boldsymbol{Y}$ and $\boldsymbol{Z}$, respectively. As established above, that $\boldsymbol{Y}$ lies in $\mathcal{N}(\boldsymbol{M})$ yields the orthogonality (9). As seen there, this gives in particular that $c_h = 0$. Next, the formula $\boldsymbol{KY} = \boldsymbol{MZ}$ may be converted into a functional form

$$\forall \varphi_h \in V_h, \qquad k_*(c_h, \varphi_h) + a_r(b_h, \varphi_h) = (\chi_h, \varphi_h).$$

Owing to the fact that c_h vanishes identically and choosing $\varphi_h = b_h$ ends to

$$a_r(b_h, b_h) = (\chi_h, b_h).$$

Now, since $\chi_h \in H_h$, calling for (9), we derive that $a_r(b_h, b_h) = 0$. This provides that $b_h = 0$ and concludes to $\boldsymbol{Y} = 0$. An immediate consequencer is that $N = 0$. Finally, the dimension m of the nilpotent matrix N in (8) coincides with the dimension of $\mathcal{N}(\boldsymbol{M})$ which is one. The proof is complete.

The analysis concludes to the fact that the differential algebraic problem (8) obtained by the space discretization of the inverse problem (1) and (4) may not be solved for arbitrary data $\boldsymbol{Y}_0$ and $\boldsymbol{G}$. The solvability requires a particular compatibility between these data. The initial state $\boldsymbol{Y}_0$ and the source data $\boldsymbol{G}(0)$ should be consistent. However, when it comes to the identifiability, the following uniqueness result holds

The semi-discrete problem (7) *has at most one solution. Existence is secured only for consistent data* $(b_{0,h}, c_{0,h})$ *and* (f, g).

5 Euler Time Scheme.

Numerical solvers for differential algebraic equation, commonly called descriptor space-state systems, is a sensitive issue especially for high (Kroenecker) indexed equations. Time schemes carelessly used for these equations may converge poorly or not at all. A specialized literature can be found in (see [13, 12, 3]). The situation is not that complicated in our case. The Kroenecker index of problem (7) is low as it equals one and the algebraic part of problem (8) is of dimension one. So to say, we profoundly doubt that it conceals any worthy information. Its main influence seems to maintain the ill-posedness for the semi-discrete problem. Thus, all the care should be paid for the

approximation of the ordinary differential (part of the equation. The concern for practitioners is possibly the consistency of the initial value and the source data which is not an easy matter because of the implicit form of differential algebraic equation. Because of the one-index of our problem it can be handled numerically using modified standard integration methods.

When the full approximation of variational problem (7) is pursued, a time marching scheme has to be combined with the finite element method. Let then τ be time step, $T = p^*\tau$ and p is the current time level. We consider $((b_h)^p, (c_h)^p)$, the space/time approximation of $(b(p\tau,\cdot), c(p\tau,\cdot))$. BDF methods , for Backward Differential Formula, are well suited to differential algebraic equations. We opt for the one step scheme which coincides with the better backward Euler first order time scheme. The variational problem to solve is thus expressed as follows: *find the sequence* $((b_h)^p, (c_h)^p)_{0\le p\le p^*}$ *that satisfy the induction*

$$\begin{aligned}
&\forall \psi_h \in H_h, \qquad \Big(\frac{(b_h)^{p+1} - (b_h)^p}{\tau}, \psi_h\Big) + k(\psi_h, (b_h)^{p+1}) = (f^{p+1}, \psi_h),\\
&\forall \varphi_h \in V_h, \qquad \Big(\frac{(c_h)^{p+1} - (c_h)^p}{\tau}, \varphi_h\Big) + k_*((c_h)^{p+1}, \varphi_h) + a_r((b_h)^{p+1}, \varphi_h) = (g^{p+1}, \varphi_h),\\
&\qquad\qquad (b_h)^0 = b_{0,h}, \quad (c_h)^0 = c_{0,h}.
\end{aligned} \tag{14}$$

The well definiteness of the sequence $((b_h)^p, (c_h)^p)_{0\le p\le p^*}$ remains questionable. We need to know if the induction defines without unambiguity $((b_h)^p, (c_h)^p)_{0\le p\le p^*}$. To clarify this point, we need to look how the time scheme is echoed on the differential algebraic equation (8),

$$\begin{aligned}
(\lambda \boldsymbol{M} + \boldsymbol{K})\boldsymbol{Y}^{p+1} &= \boldsymbol{G}^{p+1} + \lambda \boldsymbol{M}\boldsymbol{Y}^p,\\
\boldsymbol{Y}^0 &= \boldsymbol{Y}_0.
\end{aligned} \tag{15}$$

The parameter λ is the inverse of the time step, that is $\lambda = \tau^{-1} > 0$. Following Remark 4.2, the matrix $(\lambda \boldsymbol{M} + \boldsymbol{K})$ is invertible and the sequence $((b_h)^p, (c_h)^p)_{0\le p\le p^*}$ is therefore uniquely constructed. The resulting algebraic system has to be solved repeatedly and we choose to use a direct algorithm. Moreover, if one is concerned with the accuracy of the scheme, we recall that given that the Kroenecker index one, then the Euler time scheme is consistent with order one provided that the data are consistent.

6 Numerical Investigation

We investigate some features of the semi-discrete and full-discrete versions of the oxygen balance inverse problem (1) and (4). We first address the issue of determining the Kronecker index. Then, we assess through some judicious examples the reliability of the Euler scheme/mixed finite element method discussed here. Computations are realized in `Matlab`. Scripts for one dimensional finite elements are specifically implemented for our purpose.

6.1 *Eigenvalues of the pencil* $(\boldsymbol{M}, \boldsymbol{K})$

As proved above the Kronecker index and the dimension of the matrix N in formula (11) are equal to one. We assess these results numerically. Recall that the spectral decomposition of the matrix $(\boldsymbol{K}^{-1}\boldsymbol{M})$ provides necessary knowledge to learn about these indices.

We run several examples, where Cauchy's boundary conditions are prescribed on the density c at the extreme-point $x = 0$. The density b is free of any boundary condition. In the first examples, we fix different physical parameters to unity. In the others they are space varying. They are depicted in left plot in Fig. 3. We construct the finite element matrices $\boldsymbol{M}$ and $\boldsymbol{K}$ using grids with number of elements, $n = 10, 20, 30, 40$ or 50. We use both uniform grids or refined ones at the extremities as shown in the right diagram of Fig. 3.

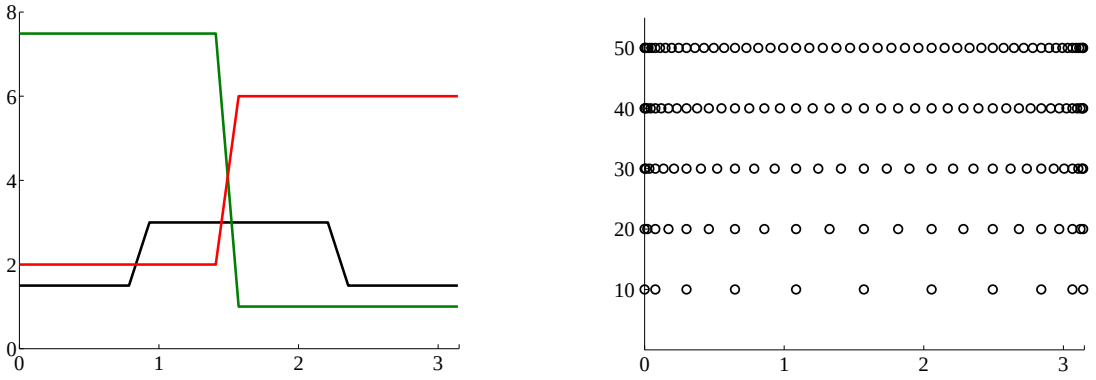

Figure 3: Space-varying parameters d (black), r (green) and r_* (red). Non-uniform grids.

The generalized eigenvalue of $\boldsymbol{M}$ with respect to $\boldsymbol{K}$ are therefore evaluated by means of the `Matlab` procedure `eig`. These eigenvalues coincides with those of $(\boldsymbol{K}^{-1}\boldsymbol{M})$. The first thing we learn from the computations is that $(\boldsymbol{K}^{-1}\boldsymbol{M})$ is diagonalizable in $\mathbb{C}$. Some eigenvalues are real, others are complex. The set of eigenvalues is symmetric with respect to the real axis which is expected given that $(\boldsymbol{K}^{-1}\boldsymbol{M})$ is a real matrix. These eigenvalues are accumulated around zero. This can be explained by the fact that $\boldsymbol{K}$ is the finite element representation of a second order operator while $\boldsymbol{M}$ is mass matrix that describes a zero-degree operator. The matrix $(\boldsymbol{K}^{-1}\boldsymbol{M})$ may be viewed as the discretization of a compact operator.

Now, we come to the key point of the Kronecker index. Results by `Matlab` confirms that 0 is an eigenvalues and it is simple. To be convinced we display in Table 1, the modulus of the eigenvalue that is the most close to zero. The algebraic multiplicity is thus one and so is the geometric multiplicity. As a result the dimension of nilpotent matrix N in the canonical Weierstrass-Kronecker form is one; actually it is identically zero. The Kronecker index is hence one, $\mu = 1$.

$n=$	10	20	30	40	50	Grids
$(d,r,r_*)=(1,1,1)$	8.3	2.0	0.9	0.5	0.3	Uniform
$(d,r,r_*)=(1,1,1)$	1.1	0.72	0.14	0.045	0.018	Non-uniform
Varying (d,r,r_*)	0.75	0.048	0.0095	0.0030	0.0012	Non-uniform

Table 1: The modulus of the smallest non-vanishing eigenvalue ($\times 10^3$).

6.2 *The inverse problem*

We use the dissolved oxygen balance model for the study of the state of a portion of a stream-water with a length $L = 2500$ meters. This portion is contaminated by some organic polluting load $\eta(t) = b(0,t)$ at the outfall point $x = 0$. Ultimately we need to quantify this time-varying density $\eta(\cdot)$. The way to achieve this consists in collecting measurements on the dissolved oxygen at $x = 0$ during two days, that is $T = 48 \times 3600$ seconds. Then we tackle computationally the inverse problem exposed above to reconstruct the BOD load $\eta(t)$ using the observations of the DO profile $\alpha(t) = c(0,t)$ at the same extreme-point $x = 0$. Let us remark that in this prospecting work the 'observed' function $\alpha(\cdot)$ is in reality synthesized. The BOD load $\eta(\cdot)$ being known, the function $\alpha(t)$ is obtained after numerically solving the well posed direct BOD-DO problem (1) and (2). A contrario, we will use this 'observed function' for the re-constitution of $\eta(t)$ by dealing with the inverse problem. In Figure 4, both functions are depicted, one, $\eta(\cdot)$, in the left diagram and the other, $\alpha(\cdot)$, in the right plot. Throughout the simulations, our choice for the physical parameters is as follows

$$r = 0.3 \times 10^{-4}\, s^{-1}, \qquad r_* = 0.6 \times 10^{-4}\, s^{-1},$$
$$v = -0.1\, m s^{-1}, \qquad d(x) = \frac{1}{40}\left(\frac{50 + 7.5 \times 10^{-4} x}{1.0 + 1.5 \times 10^{-4} x}\right)^2 m^2 s^{-1}.$$

Symbols m and s are for meter and second. The space dependent dispersion $d = d(x)$ is varying increasingly in the interval $[34.2975, 35.5837]$. We refer for instance to [20] for very close values to these.

We start the computational runs with a noise-free DO profile $\alpha(\cdot)$, the one represented in Figure 4. The approximated organic waste load $\eta_D(\cdot)$ ([1]) at $x = 0$, obtained by solving the discrete inverse problem (15), is then plotted in red symbols $\circ$ in the left panel of Figure 4. It can be noticed that the density $\eta_D(\cdot)$ simulated numerically seems in a perfect agreement with the exact one. This is an evidence, if need be, of the fitting of the mixed formulation to the inverse problem (1) and (4). indeed, the resulting variational problem (14) provides satisfactory results.

More numerical experimentations are realized when the observation $\alpha(\cdot)$ is perturbed with an

[1] The index $_D$ is for discrete.

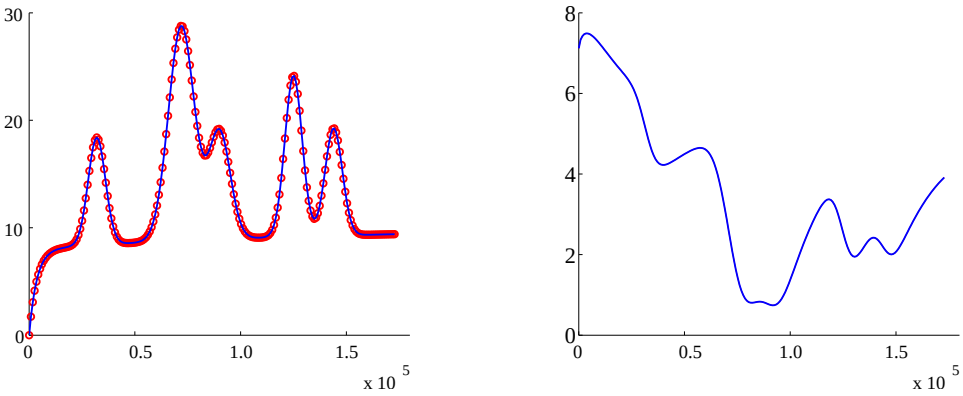

Figure 4: BOD load $\eta(\cdot)$ (left) and DO profile $\alpha(\cdot)$ (right).

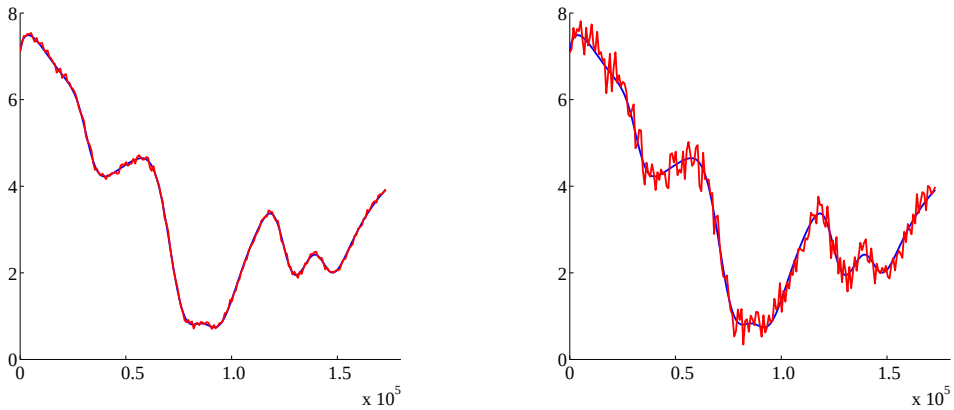

Figure 5: Noisy DO profiles —variance $\sigma = 0.05$ (left) and $\sigma = 0.25$ (right)—

additional white Gaussian noise with variances $\sigma = 0.05$ and $\sigma = 0.25$. Noisy profiles are superimposed with the exact one in Figure 5. Crude computations are thus carried out. No regularization is introduced and no preparation is made to correct the data inconsistency the noise may create. Noise is expected to ruin the numerical solution. That is what exactly happen; facts can be checked out in the plots of Figure 6. If the magnitude of the white noise grows higher then the computed solution seems to behave in completely erratic way and is far away from the exact 'real' polluting load as a time dependent function.

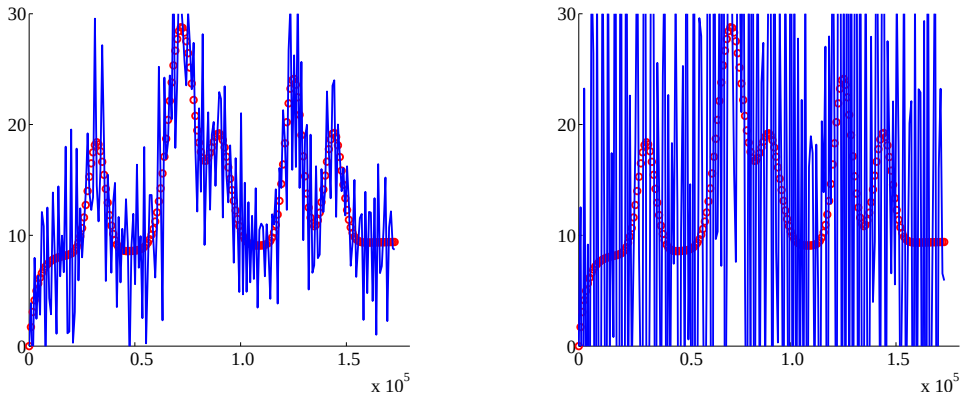

Figure 6: Computed BOD loads for noisy data.

A possible remedy to restore a reasonable load is to apply a-posteriori Gaussian filter to dampen the harmful effect of noise on the load function (see [2]). The a-priori unrecognizable and apparently inaccurate computed function $\eta_D(\cdot)$ conceals an effective signal. Indeed, that hidden signal can then be reconstructed after operating the filter on the approximated profile. Figure 7 depicts the filtered signals. They reproduce the main features of the exact profile in particular the number of peaks and dips. These are interesting information to hydrological engineers, especially in facing accidental spills in the stream waters.

The last issue assessed here is the impact on computations of noise presence on the initial condition $c_0(\cdot)$. An example is run in the case where $c_0(\cdot)$ is contaminated by white Gaussian noise of variance $\sigma = 0.5$. Both noisy initial data and the computed BOD load are portrayed in Figure 8. Letting aside a visible effect at the initial instant, the profile of $\eta(\cdot)$ seems to be nicely approximated. The observation may be put in relation with the inconsistency of the noisy initial data wit the boundary condtions at the outfall point. Using a Gaussian filter is liable to bring some correction to the signal and repair that deviation a the vicinity of $t = 0$.

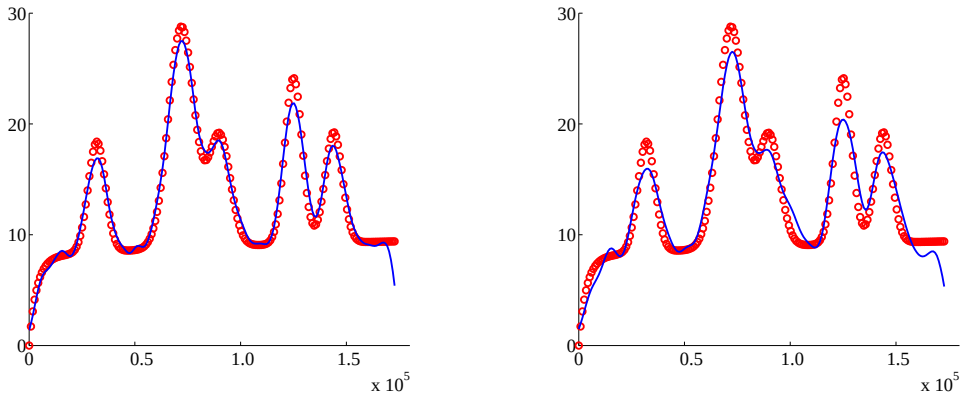

Figure 7: Computed BOD loads at the outfall point after applying a Gaussian filter.

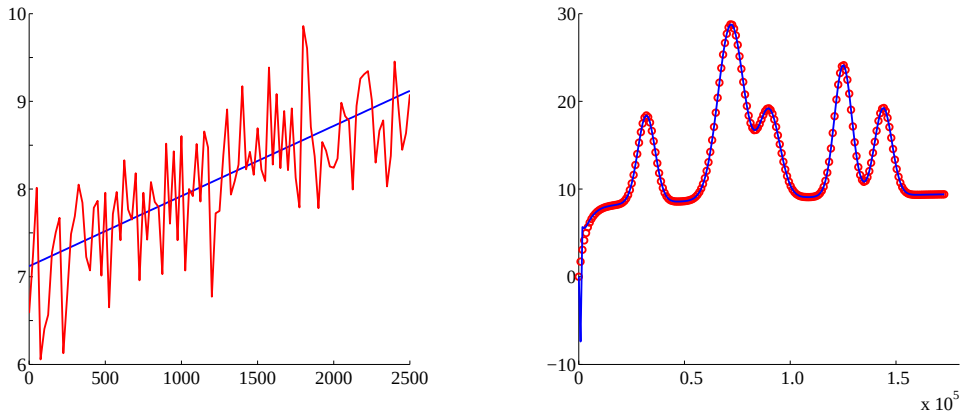

Figure 8: Noisy $c_0(\cdot)$ (left). Computed polluting load $\eta_D(\cdot)$ (right).

7 Conclusion

The relevance of the mixed finite element method for the boundary data completion in the dispersive BOD-DO model is the main purpose we pursue in both mathematical and computational grounds. The semi-discrete problem we obtain turns out to be a differential algebraic equation (DAE). Tools specifically developed for implicit DAE enable a careful analysis of the semi-discrete equations. As result, we highlight the reason why existence fails for some (inconsistent) data. Prospective numerical experiments presented show the liability of such a finite element approximation when combined with a well adapted time marching scheme in solving the inverse problem we cope with. Further research in many directions is under consideration. Extension to higher dimension, using less naive filters, testing and sorting different regularization strategies are all in expected in the forthcoming work. The analysis of the inverse problem where measurements on the DO density are not accessible at the outfall point is also under consideration.

References

[1] Ben Belgacem, F. Uniqueness for an ill-posed reaction-dispersion model: Application to organic pollution in stream-waters. *Inverse Problems and Imaging*, 6 (2012), 163 – 181.

[2] Blinchikoff, H., and Zverev, A. *Filtering in the time and frequency domains.* Classic series. Noble Publishing, 1976.

[3] Brenan, K., Campbell, S., and Petzold, L. *Numerical Solution of Initial-Value Problems in Differential Algebraic Equations, Classics in Applied Mathematics*, vol. 14. SIAM, Philadelphia, PA,, 1996.

[4] Brenner, S. C., and Scott, L. R. *Mathematical Theory of Finite Element Methods. Texts in Applied Mathematics,*, vol. 15. Springer Verlag, New-York, 1994.

[5] Brown, L. C., and Barnwell, T. O. *The Enhanced Stream Water Quality Models QUAL2E and QUAL2E-UNCAS: Documentation and User Manual.* Environmental Protection Agency, 1987.

[6] Ciarlet, P.-G. *The Finite Element Method for Elliptic Problems.* North Holland, 1978.

[7] Dostanic, M. R., , and Milinkovic, D. Z. Asymptotic behavior of singular values of certain integral operators. *Publications de l'institut mathématique, nouvelle série, 74* (1996), 83–98.

[8] Griepentrog, E., and März, R. *Differential-Algebraic Equations and Their Numerical Treatment, Teubner-Texte zur Mathematik*, vol. 88. Leipzig,, 1986.

[9] Gripenberg, G., London, S. O., and Steffans, O. *Volterra Integral and Functional Equations.* University Press, Cambridge, 1990.

[10] Jolánkai, G. *Basic river water quality models : computer aided learning* (CAL) *programme on water quality modelling* (WQMCAL). International Hydrological Programme. UNESCO document 121363, Paris, 1997.

[11] Kronecker, L. Gesammelte werke, Reduktion der scharen bilinearer formen. *Akad. d. Wiss. Berlin, Volume III* (1890), 141–155.

[12] Kunkel, P., and Mehrmann, V. *Differential-Algebraic Equations. Analysis and Numerical Solution, in EMS Textbooks in Mathematics.* European Matematical Society, Zürich,, 2006.

[13] Lamour, R., März, R., and Tischendorf, C. *Differential-Algebraic Equations: A Projector Based Analysis, in Differential-Algebraic Equations Forum.* Springer, Heidelberg New York Dordrecht London, 2013.

[14] Lions, J. L., and Magenes, E. *Problèmes aux Limites Non Homogènes et Applications*, vol. 2. Dunod, 1968.

[15] Okubo, A. *Diffusion and Ecological Problems: Mathematical Models*. Springer-Verlag, 1980.

[16] Pazy, A. *Semigroups of Linear Operators and Applications to Partial Differential Equations*. Springer-Verlag, 1983.

[17] Riaza, K. *Differential-Algebraic Systems: Analytical Aspects and Circuit Applications*. World Scientific Publishing,, 2008.

[18] Rubin, H., and Atkinson, J. *Environmental Fluid Mechanic*. Marcel Dekker, New York, 2001.

[19] Streeter, H., and Phelps, E. A study of the pollution and natural purification of the Ohio river. *US Public Health Bull. 146* (1925).

[20] Tyagi, B., Gakkhar, S., and Bhargava, D. Mathematical modelling of stream do-bod accounting for settleable bod and periodically varying bod source. *Environmental Modelling & Software 14*, 5 (1999), 461–471.

[21] Vejchodský, S. Necessary and sufficient condition for the validity of the discrete maximum principle. *Proceedings of ALGORITMY* (2012), 311–320.

[22] Wahba, G. *Ill posed problems: Numerical and statistical methods for mildly, moderately and severely ill posed problems with noisy data.* University of Wisconsin, Madison. Unpublished proceedings of the Delaware Conference on Ill Posed Inverse Problems, TR 595, 1980.

[23] Weierstrass, K. Gesammelte werke, Zur theorie der bilinearen und quadratischen formen,. *Akad. d. Wiss. Berlin, Volume II* (1868), 19–44.